IEEE Sensors Council IEEE SENSORS JOURNAL, VOL. XX, NO. XX, XXXX 2022

Microwave Rotation Sensor Based on Reflection Phase in Transmission Lines Terminated with Lumped Resonators

Zahra Mehrjoo, *Student Member, IEEE*, Amir Ebrahimi, *Member, IEEE*, Grzegorz Beziuk, *Member, IEEE*, Ferran Martín, *Fellow, IEEE*, Kamran Ghorbani, *Senior Member, IEEE*

***Abstract*— A phase variation-based rotation sensor is presented in this paper. The sensor is realized using a semi-circular bent coplanar waveguide (CPW) terminated with a stepped impedance LC resonator. A circular dielectric slab is rotating above the resonator. Rotation of the slab modifies the overall capacitance and thus the input impedance of the resonator. This, in turn, modifies phase of the reflection coefficient, which is translated to the rotation angle. The sensor's linearity is eventually enhanced by tapering the width of the capacitive metallic patch along the rotation direction. The operation and sensing performance is studied in detail, using a circuit-based analysis and electromagnetic simulations. The designed sensor is capable of detecting the direction of rotation. A sensor prototype is fabricated and experimentally measured to prove the developed design and analysis procedure.**

***Index Terms*— Microwave sensors, phase variation sensors, reflective mode sensors, rotation sensors.**

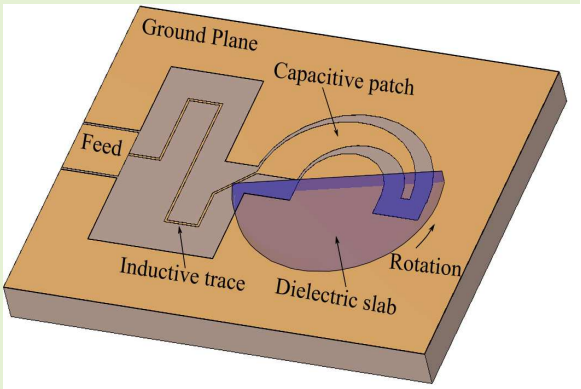

I. Introduction

MEASURING and detection of lateral and rotational displacements are of especial interest in various scientific and industrial applications such as robotics, industrial automation, advanced manufacturing, space observation, etc. [1]. The conventional technologies for detecting lateral and angular displacements are capacitive [1], [2], magnetic [3]–[5], resistive [6], optical [7], [8], and microwave methods [9]. Due to the potential passive operation, real-time response, and low-cost implementation, microwave sensors have found widespread adaptation in various instrumentation and measurement applications. In comparison to the optical counterparts, microwave sensors show high robustness to harsh environments [10]–[12] and are more compatible with electronic integration technologies such as, low temperature cofired ceramic (LTCC) and micro-electromechanical (MEMs). Metamaterials-inspired elements, such as, split-ring resonators (SRRs) and their complementary counterparts CSRRs [13]–[15], electric-LC (ELC) and magnetic-LC (MLC) resonators [16], were utilised as building blocks in the design of such sensors leading to enhanced sensitivity and compact sizes. According to the magnetic or electric nature of the coupling between these resonators and transmission lines and waveguides, alteration in the sensing variable modifies the device S-parameters. Theses changes are then processed and translated to the sensing parameter [17]–[20]. These sensors are used in applications such as environmental monitoring [21], [22], detection of gaseous [23]–[26] and fluidic agents [27]–[33] and measurement of physical displacement [34]–[36] and rotation [37]–[42].

Microwave rotation sensors can be categorized as three main groups, according to the operation mode. The first group is the frequency shift sensors [39]–[43]. The second group includes the notch depth detection sensors [44]–[47], and the third group consists of the phase variation sensors [48]–[58]. In the sensors where the frequency shift is the measurement variable, two coupled resonators are moved with respect to each other, resulting in a shift of the resonance frequency. An advantage of these sensors is the high immunity to noise [9]. Notch depth variation sensors form the second category. The sensing principle in these sensors is the alignment between the resonators and the transmission line. Breaking the symmetric alignment through rotation excites the resonator producing a notch in the sensor response, where the notch depth is a function of the rotation angle. This type of sensors are more robust to the

Zahra Mehrjoo, Amir Ebrahimi, Grzegorz Beziuk, and Kamran Ghorbani are with the School of Engineering, Royal Melbourne Institute of Technology (RMIT University), Melbourne, VIC 3001, Australia (e-mail: zahra.mehrjoo@student.rmit.edu.au).

Ferran Martín is with the GEMMA/CIMITEC, Departament d'Enginyeria Electrònica, Universitat Autònoma de Barcelona, 08193 Barcelona, Spain (e-mail: ferran.martin@uab.es). This work was supported by MINECO-Spain under Project PID2019-103904RB-I00, in part by the Generalitat de Catalunya under Project 2017SGR-1159, in part by the Institucio ´ Catalana de Recerca i Estudis Avançats (who awarded Ferran Martín), and in part by the FEDER funds.

variation of the environmental changes such as temperature. Meanwhile, interferences and noise might induce error in the notch depth variations. One main advantage of these sensors is the single frequency detection, which provides simplicity in the measurement setup compared to their frequency shift counterparts [59]. The third category are the phase variation sensors. Similar to the frequency variation sensors, the phase variation sensors offer high robustness with respect to noise and interferences. Furthermore, they offer simple and low cost measurement because of their single frequency operation. Recently, phase variation sensors were adopted for materials characterization and measuring physical displacements [48], [50]–[57]. In material characterization sensors, loading the material-under-test (MUT) on transmission line or a resonator-loaded waveguide modifies the S-parameter phase. The measured phase variation is processed and used for characterization of the electromagnetic properties of the MUT. Recently, phase variation rotation sensors were developed in [55], [58]. The sensor in [55] is designed using SRR-loaded slot line, where rotating the SRR with respect to the symmetry line causes a phase difference between the reflection coefficients at the two ports of the sensor. The dynamic range is enhanced up to 360° by adding a flag resonator and performing the measurement at two different frequencies. The sensor in [58] is designed using an asymmetrical CSRR resonator loaded on a microstrip transmission line. Likewise, the operation principle is based on the phase difference between the reflection coefficients of the in/output ports. Despite a wide dynamic range, these sensors require two port measurement and then calculation of the phase difference between the reflection coefficient of the two ports at two different frequencies.

Here, we propose a phase variation rotation sensor offering single frequency and single port measurement, where the rotation is directly inferred from the reflection coefficient phase without the requirement of any further processing/calculation. The sensor consists of a CPW terminated with a semi-lumped LC resonator, where the capacitance is implemented using a tapered metallic patch and a rotational dielectric slab above the resonator. The tapering approach offers a linear phase variation for different rotation angles. The sensor covers rotation angles up to 180°.

The rest of this paper is organized as follows: the circuit-based analysis and design procedure are discussed in Section II. Section III validates the developed rotation sensing concept through fabrication of a sensor prototype and experimental measurements. Finally, Section IV provides the conclusion.

II. Sensor Operation Principle and Analysis

A layout of the proposed phase variation rotation sensor is shown in Fig. 1 with both top and side views. In addition, an equivalent circuit model of the sensor is given in Fig. 2. The sensor is implemented using a 50 Ω coplanar waveguide (CPW) terminated to a semi-lumped LC resonator. A meandered metallic trace of width t is used to form the inductance. The capacitance is created using a semi-circular patch as shown in Fig. 1(a), where C is the edge

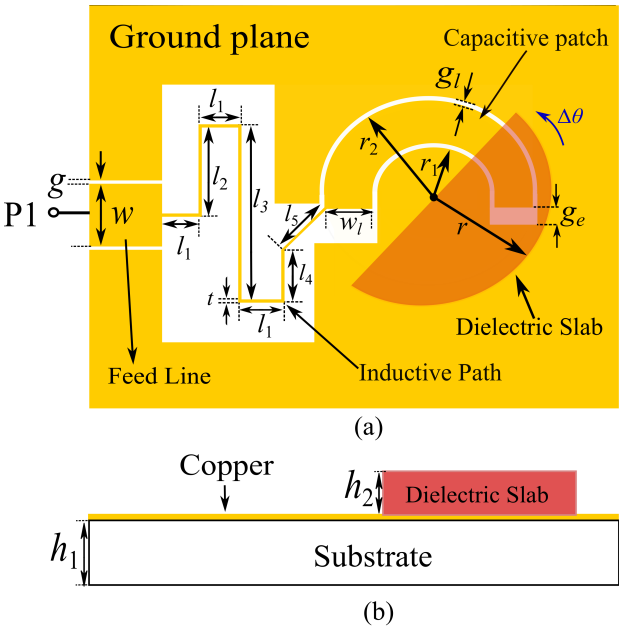

Fig. 1. Schematic view of the proposed phase variation rotation sensor. (a) Top view. (b) Side view. The yellow color indicates the metallization layer. Dimensions are: w = 4.8 mm, w_l = 3.71 mm, g = g_l = 0.2 mm, t = 0.2 mm, l_1 = 3.2 mm, l_2 = 6.6 mm, l_3 = 12.80 mm, l_4 = 3.6 mm, l_5 = 3.94 mm, r_1 = 4 mm, r_2 = 8 mm, r = 9 mm, h_1 = 3.175 mm and h_2 = 1.28 mm.

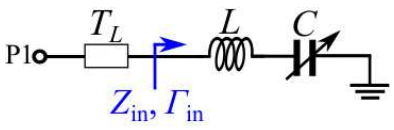

Fig. 2. Eqiuvalent circuit model of the proposed sensor.

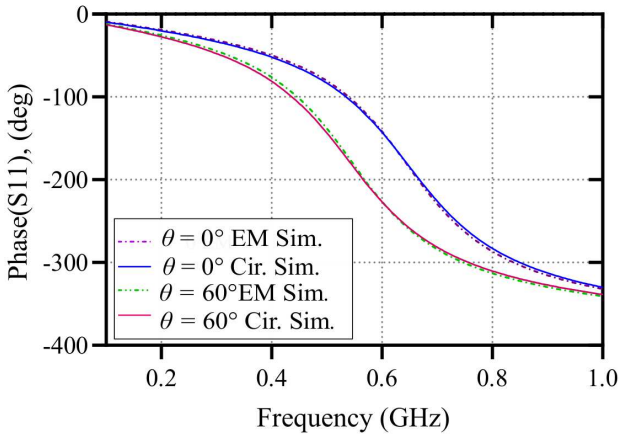

Fig. 3. Comparison between the full-wave EM and circuit model simulation results of the sensor. The circuit parameters are L = 29.4 nH and C = 2 pF for θ = 0° and C = 2.82 pF for θ = 60°.

capacitance between the patch and the CPW ground plane. A rotatable half circular dielectric slab is placed above the patch capacitor. By rotating the dielectric slab, the overlapping area between the patch and the slab is modified, causing a change in the effective permittivity around the patch. Consequently, the total capacitance of the structure is changed, modifying the input impedance (Z_{in}). This causes a variation in the

phase of reflection coefficient, which can be translated to the rotation angle. In order to validate the lumped circuit model in Fig. 2, the circuit parameters have been calculated for two typical rotation angles of 0° and 60°. Fig. 3 presents a comparison between the circuit model and the full-wave simulation results of the sensor for the two rotation angles. The circuit simulation is performed using Keysight ADS and full-wave electromagnetic (EM) simulations are performed using the CST Microwave Studio. The good agreement between the results in Fig. 3 validates the circuit model. The sensor is designed using a Rogers RT5880 substrate with a thickness of 3.175 mm, $\varepsilon_r = 2.2$ and $\tan\delta = 0.0009$. The rotating dielectric slab is Rogers RO3006 with 1.28 mm thickness, $\varepsilon_r = 6.5$ and $\tan\delta = 0.002$.

A. Analysis of the proposed sensor

Here, we analyze the sensitivity of the sensor and prove that the sensitivity is a nonlinear function of rotation. The input impedance (Z_{in}) of the lumped LC resonator in Fig. 2 is defined as

$$Z_{\text{in}} = j\omega L + \frac{1}{j\omega C}. \tag{1}$$

When the dielectric slab is rotated, part of the capacitive patch is loaded by the dielectric and, the overall capacitance is increased to $C' = C + \Delta C$. Thus, the new input impedance would be

$$Z_{\text{in}} = j\omega L + \frac{1}{j\omega C'} = \frac{1-\omega^2 LC'}{j\omega C'}. \tag{2}$$

Suppose that $\omega_0 = \frac{1}{\sqrt{LC}}$, then we can write:

$$Z_{\text{in}} = \frac{1-\frac{\omega^2}{\omega_0^2}(1+\frac{\Delta C}{C})}{j\omega C(1+\frac{\Delta C}{C})}. \tag{3}$$

On the other hand, the reflection coefficient Γ_{in} is defined as:

$$\Gamma_{\text{in}} = \frac{Z_{\text{in}} - Z_0}{Z_{\text{in}} + Z_0}. \tag{4}$$

By introducing (3) in (4) and after some simplifications, phase of the reflection coefficient can be calculated as:

$$\phi_{\text{in}} = -2\arctan\left(\frac{1}{Z_0\omega C(1+\frac{\Delta C}{C})} - \frac{\omega}{Z_0\omega_0^2 C}\right). \tag{5}$$

The phase sensitivity with respect to the rotation angle (θ) is defined as

$$S = \frac{d\phi_{\text{in}}}{d\theta} = \frac{d\phi_{\text{in}}}{dC'}\frac{dC'}{d\theta} = \frac{d\phi_{\text{in}}}{d\Delta C}\frac{d\Delta C}{d\theta}. \tag{6}$$

The first term in (6), can be calculated as:

$$\frac{d\phi_{\text{in}}}{d\Delta C} = \frac{2}{Z_0\omega C^2\left(1+\frac{\Delta C}{C}\right)^2} \times \frac{1}{1+\left(\frac{1}{Z_0\omega C(1+\frac{\Delta C}{C})} - \frac{\omega}{Z_0\omega_0^2 C}\right)^2} \tag{7}$$

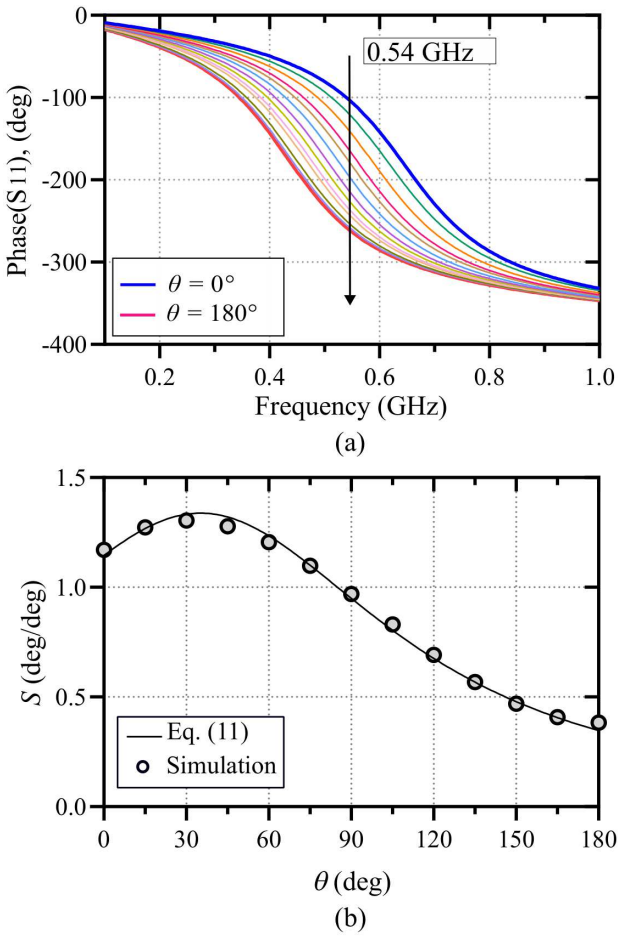

Fig. 4. Full-wave simulation results of S_{11} phase for the sensor in Fig. 1, for different rotations from 0° to 180° with the step size of 15°.

and, after simplification

$$\frac{d\phi_{\text{in}}}{d\Delta C} = \frac{2Z_0\omega_0^4\omega}{Z_0^2\omega^2C^2\omega_0^4\left(1+\frac{\Delta C}{C}\right)^2 + \left((1+\frac{\Delta C}{C})\omega^2 - \omega_0^2\right)^2}. \tag{8}$$

To determine the second term in (6), we should consider that the capacitance C is the gap capacitance between the circular patch of the LC resonator and the ground plane. The overall capacitance of the unloaded patch is C. If part of the patch is covered by the rotatable slab as a function of rotation (θ), the total capacitance of the resonator will be increased by [60]

$$\Delta C = C\frac{\theta}{\pi}\frac{\varepsilon_s - 1}{\varepsilon_r + 1}, \tag{9}$$

where ε_r represents the relative permittivity of the sensor substrate and ε_s is the relative permittivity of the rotatable slab. This equation (9) is valid if the gap width between the capacitive patch and ground plane is much smaller than the the capacitive patch width ($\frac{w_l}{g_l} > 10$) [60]. Based on (9), we can write

$$\frac{d\Delta C}{d\theta} = \frac{C}{\pi}\frac{\varepsilon_s - 1}{\varepsilon_r + 1} = kC. \tag{10}$$

TABLE I
CASES FOR VERIFICATION OF THE DESIGN PROCEDURE.

Case No.	f(GHz)	C(pf)	C_{180}(pf)	β	f_0(GHz)	L(nH)
1	0.54	2	5.66	2.83	0.705	25.474
2	1.1	1.2	3.8	3.166	1.512	9.232
3	2.5	0.5	3	6	3.956	3.236

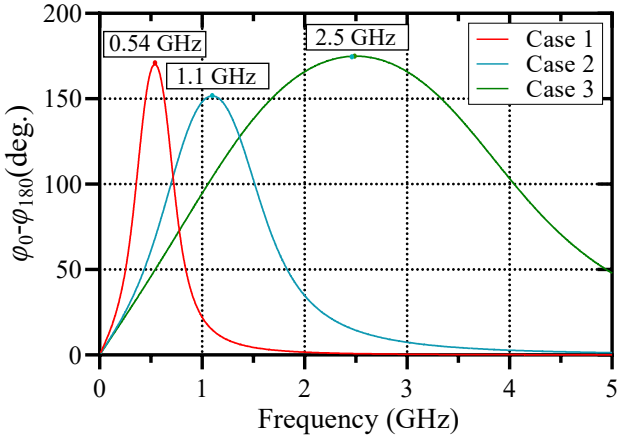

Fig. 5. Reflection phase difference between $\boldsymbol{\theta = 0°}$ and $\boldsymbol{\theta = 180°}$ for three circuit level cases in Table I, for verification of the theoretical analysis.

As a result, by substituting (8) and (10) in (6), the sensitivity is calculated as

$$S = \frac{2Z_0\omega_0^4\omega kC}{Z_0^2\omega^2C^2\omega_0^4(1+k\theta)^2 + \left((1+k\theta)\omega^2 - \omega_0^2\right)^2}. \quad (11)$$

Based on (11), the sensitivity is a function of frequency and rotation angle (θ). The sensitivity decreases for larger rotation angles. In order to validate such an analysis, the phase variations of a typical sensor with the dimensions given in Fig. 1 are obtained as a function of rotation using full-wave simulations in the CST Microwave Studio. The full-wave simulation results are plotted in Fig. 4(a). Furthermore, the sensitivity as a function of the rotation angle (θ) at a fixed measurement frequency of 0.54 GHz is calculated using (11) and the resulting curve is compared with sensitivities obtained based on the full-wave simulations in Fig. 4(b). The close agreement between the results in this figure confirms the analysis and the sensitivity predicted by (11). In this sensor, we measure the phase variation at 0.54 GHz, where the maximum phase variation happens within ($0°-180°$) rotation range. Such a frequency will be analytically calculated in this section. In order to find the frequency that maximizes the sensitivity, we take the derivative of (9) with respect to ω and force the result to zero. By doing so, the resulting equation will be biquadratic in terms of ω and can be expressed as

$$3\alpha\omega^4 + \left(Z_0^2C^2\omega_0^4\alpha^2 - 2\alpha\omega_0^2\right)\omega^2 - \omega_0^4 = 0, \quad (12)$$

where $\alpha = 1 + k\theta$ is the ratio between the total capacitances for $\theta°$ and $0°$ rotations. Solving the above equation results in

$$\omega^2 = \frac{2\alpha\omega_0^2 - Z_0^2C^2\omega_0^4\alpha^2 + \sqrt{\left(2\alpha\omega_0^2 - Z_0^2C^2\omega_0^4\alpha^2\right)^2 + 12\alpha^2\omega_0^4}}{6\alpha^2}. \quad (13)$$

Equation (13) maximizes the sensitivity around a specific rotation angle of θ. However, to obtain a maximum dynamic range ($180°$), we are interested to have the maximum phase variation between the start ($\theta = 0°$) and the end ($\theta = 180°$) rotation angles. In order to achieve this goal, the $\phi_{\text{in}}(180°) - \phi_{\text{in}}(0°)$ should be maximized. Based on (5), we have

$$\phi_{\text{in}}(180°) = -2\arctan\left(\frac{1}{Z_0\omega C\beta} - \frac{\omega}{Z_0\omega_0^2 C}\right), \quad (14)$$

and

$$\phi_{\text{in}}(0°) = -2\arctan\left(\frac{1}{Z_0\omega C} - \frac{\omega}{Z_0\omega_0^2 C}\right). \quad (15)$$

In (14) we have

$$\beta = \frac{C_{180°}}{C}, \quad (16)$$

where $C_{180°}$ is the total capacitance of the LC resonator for $\theta = 180°$ and C is the total capacitance for $\theta = 0°$. These values can be estimated using (9) or more accurately determined by curve fittings between the full-wave EM simulations and circuit model simulations of a sensor with pre-assumed dimensions of the capacitive patch based on the desired final sensor size. In these simulations, arbitrary values can be considered for the inductive trace. Now, in order to find the frequency, where the maximum S_{11} phase variation occurs between the $\theta = 180°$ and $\theta = 0°$, we should solve the following equation

$$\frac{d(\phi_{\text{in}}(180°) - \phi_{\text{in}}(0°))}{d\omega} = 0. \quad (17)$$

The above equation results in (18) that is biquadratic in terms of ω and ω_0.

$$3\beta\omega^4 + \omega^2\left(\beta Z_0^2C^2\omega_0^4 - (\beta+1)\omega_0^2\right) - \omega_0^4 = 0. \quad (18)$$

By solving (18) we obtain

$$\omega^2 = \frac{\omega_0^2}{6\beta}\left(\beta + 1 - \beta Z_0^2C^2\omega_0^2 \pm \sqrt{12\beta + \left(\beta Z_0^2C^2\omega_0^2 - \beta - 1\right)^2}\right) \quad (19)$$

The ω obtained from (19) is our operation frequency (measurement frequency) since the maximum phase variation as a function of rotation between $\theta = 180°$ and $\theta = 0°$ happens at this frequency. Supposing ω as our operation frequency, resonance frequency of the LC tanks for an unloaded sensor ($\theta = 0°$) is obtained by solving (18) in terms of ω_0 as

$$\omega_0^2 = \omega^2\frac{\beta + 1 \pm \sqrt{(\beta+1)^2 - 12\beta\left(\beta\omega^2Z_0^2C^2 - 1\right)}}{2(\beta\omega^2Z_0^2C^2 - 1)} \quad (20)$$

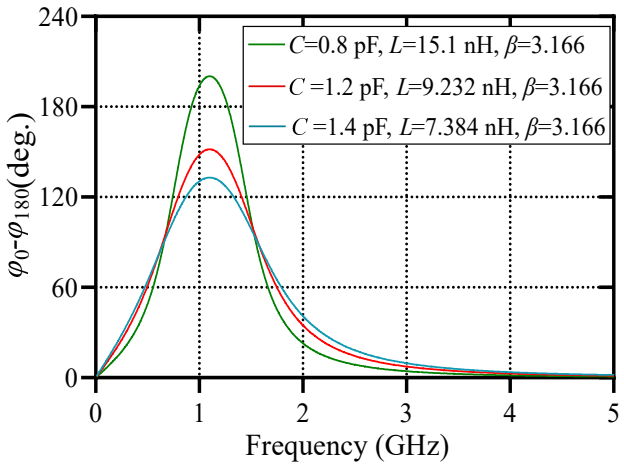

Fig. 6. Reflection phase difference between $\theta = 0°$ and $\theta = 180°$, for three different sensors operating at 1.1 GHz with $\beta = 3.166$.

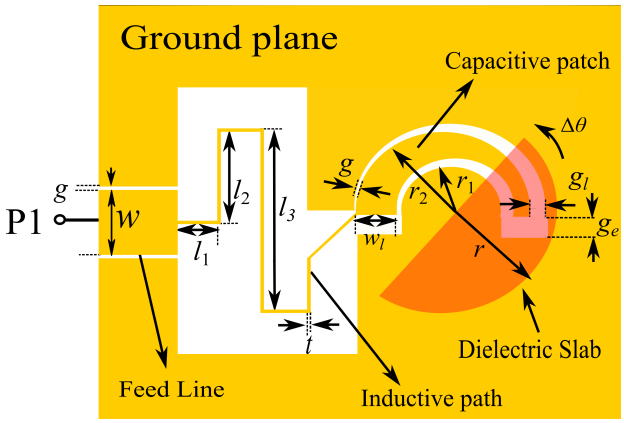

Fig. 7. Schematic view of the linearized phase variation rotation sensor. $l_2 = 6.54$ mm, $l_3 = 12.64$ and $g_l = 1.6$ mm. All other dimensions are as in Fig. 1.

In (20), the solution that returns a positive real value for ω_0 is correct. The inductance (L) value is also known after calculating the ω_0 value from (20). In order to investigate validity of (20) for design purposes, three different circuit level designs are considered and listed in Table I. In each case, the operation frequency (f), C and $C_{180°}$ are given. Then, the resonance frequency of the LC tank and L value are calculated using (20). Finally, the reflection phase difference between $\theta = 0°$ and $\theta = 180°$ are calculated and plotted in Fig. 5. Based on the curves in Fig. 5, the frequency, where the maximum phase difference between the two states happens, coincides with the pre-specified f for each case in Table I. The high agreement between the results in Fig. 5 and the specified f verifies (20).

Having a closer look into (11) reveals that the phase sensitivity has a reverse relation with C meaning that a smaller C results in a higher phase sensitivity. Thus, at a constant working frequency (f) and capacitance ratio (β), we expect that smaller C results in larger phase variation of the sensor between $\theta = 0°$ and $\theta = 180°$. This is verified by designing the circuit element values for three different example sensors operating at 1.1 GHz with $\beta = 3.166$ for all of them. The phase variation ($\Delta\phi$) of these sensors between $\theta = 0°$ and $\theta = 180°$ are simulated and plotted in Fig. 6, where they verify the above analysis. Therefore, in real designs, it is desired to have a smaller capacitance and larger inductance in the LC tank to achieve a better sensitivity. However, the achievable values of L and C are always limited by the fabrication and the used dielectric substrate.

B. Sensor Linearization

The Proposed sensor is able to measure the rotation up to $180°$. However, as proven by the sensitivity analysis and the results in Fig. 4, the phase variation saturates at high rotation angles showing a nonlinear performance of the sensor. Note that the phases are measured at a single frequency (0.54 GHz), where the phase variation is maximum between $0°$ and $180°$ rotation angles. Such a frequency was analytically calculated in the previous section. In real applications, the interest is to linearize the sensing performance to avoid saturation of the sensor phase variation at large rotation angles. Based on (11), one approach to linearize the sensor might be to decrease the k coefficient by reducing the relative permittivity of the rotatable dielectric slab (ε_s). However, this also leads to a reduced phase variation as a function of θ. A more practical implementation is to taper the width of the capacitive patch along the rotation, as shown in an improved design in Fig. 7. In such a configuration, the slot width is large at the start of rotation. This causes a smaller variation of the overall capacitance as the dielectric slab covers part of the patch at small rotation angles. On the other hand, the slot width becomes narrower towards the large rotation angles meaning the variation of the overall capacitance as a function of rotation is sharper for large θ values. This reduces the phase variation for the smaller rotation angles and enhances the phase variation for the large rotation angles leading to a linearized sensing characteristics. As demonstrated in our previous work on a resonant displacement sensor [35], larger tapering results in better linearity. The proposed linearization technique is validated by the full-wave simulation results of S_{11} phase for different rotation angles from $0°$ to $180°$ with the step size of $15°$ in Fig. 8. Fig. 9 verifies a more linear profile especially for large rotation angles achieved by tapering the capacitive patch, by comparing the sensors with $g_l = 0.2$ mm and $g_l = 1.6$ mm (the initial and linearized designs). Note that the phases for the linearized sensor are measured at a single frequency (0.68 GHz), where the phase variation is maximum between $0°$ and $180°$ rotation angles.

C. Design Procedure

Based on the modeling, analysis, and the linearization method introduced in the previous sections, here we develop a step-by-step design procedure for the proposed rotation sensor considering a pre-specified operation frequency (f). The developed design procedure is

(i) Set the operation frequency (f).

(ii) Based on the available substrate and the rotating dielectric slab, a circular patch should be designed as the capacitive part of the LC tank. The patch dimensions should be chosen

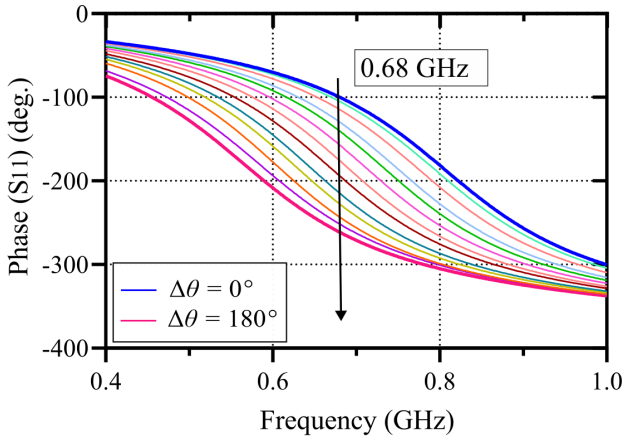

Fig. 8. Full-wave simulation results of the S_{11} phase for the linearized sensor in Fig. 7, for different rotations from $0°$ to $180°$ with the step size of $15°$.

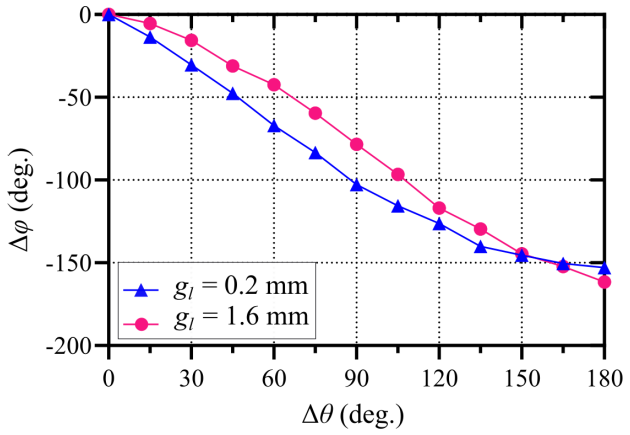

Fig. 9. S_{11} phase variation for the the senosors with g_l= 0.2 mm and g_l= 1.6 mm (the initial and linearized designs), for different rotations from $0°$ to $180°$ with the step size of $15°$.

based on the size limitation for the sensor. To achieve a linear performance, the patch should be tapered as explained in the previous section.

(iii) C_0 and C_{180} should be determined. To this aim, the patch can be simulated in series with an inductive trace with logical arbitrary dimensions and the capacitance values for $\theta = 0°$ and $\theta = 180°$ are obtained by curve fitting between the full-wave EM and circuit model simulation results.

(iv) Based on the previous step, β is calculated using (16).

(v) Now, using (20), resonance frequency of the LC tank (ω_0) is obtained together with the inductance L value. If (20) does not return a real solution, it means that it is not possible to achieve the specified operation frequency with the designed capacitive patch. Thus, the patch dimensions should be re-designed accordingly, or the operation frequency should be changed.

(vi) Dimensions of the inductive trace should be designed and fine tuned by curve fitting between the EM and circuit model simulations to meet the designed value of L in the previous step.

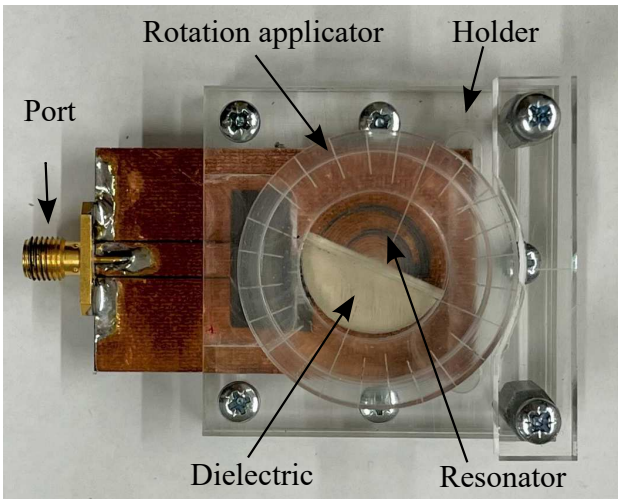

Fig. 10. The fabricated sensor prototype.

III. Experimental Validation and Results

Using the analytical design procedure developed in the previous section, a rotation sensor is designed to operate at 0.68 GHz with the layout in Fig. 7 to validate the rotation sensing concept developed in the previous sections. The sensor and the dielectric slab are fabricated using the same dielectric materials mentioned in Section II. The fabricated sensor prototype is shown in Fig. 10. A housing is designed to hold the sensor using PMMA material. The rotating part is designed using a cylinder that is marked to show the rotation angles in $15°$ steps. This cylinder is attached to the semi-circular dielectric slab using a foam spacer and can rotate the slab with respect to the capacitive patch. In each measurement step, the dielectric slab is rotated by $15°$ and the corresponding reflection phase response is measured and recorded using a vector network analyzer (VNA). The measured S_{11} phases for rotation angles from $0° - 180°$ are plotted in Fig. 11. A comparison between the simulated and measured phases at the design frequency of 0.68 GHz is presented in Fig. 12. The measurement and simulation results of phase variation are both taken at 0.68 GHz. As shown, There is a very good agreement between the simulated and measured phase variation curves, which verifies the application of the proposed rotation sensor concept and the developed design procedure.

A comparison between the designed rotation sensor and the state-of-art phase variation based rotation sensors in the literature is provided in Table II. In this table, the average sensitivity (S_{av}) is defined as

$$|S_{av}| = \frac{1}{n}\sum_{k=1}^{n}|S_k|, \tag{21}$$

where n is the number of the measured points. Both of the sensor presented in [55], [58] requires simultaneous measurement of both S_{11} and S_{22} phases for determining the rotation angle, while the presented sensor performs the measurement based on phase variation of S_{11} and using a single resonator. This significantly simplifies the design of the measurement electronics. In addition, the rotation sensor proposed in this paper offers higher sensitivity than the one in [55] and

TABLE II
COMPARISON WITH PREVIOUS PHASE VARIATION-BASED ROTATION SENSORS.

Ref.	f_0 (GHz)	$\|S_{av}\|$	Dyn. Range (°)	Elec. size (λ_g^2)	No. of Res.	Resonator Type	Operation Base
[55]	3.5	0.63	360	0.16×0.16	2	SRR	Phase of S_{11} and S_{22}
[58]	4.7	Min: 0.91, Max: 1.32	180	0.5×0.8	1	CSRR	Phase of S_{11} and S_{22}
T.W	0.68	1.03	180	0.05×0.14	1	SIR	Phase of S_{11}

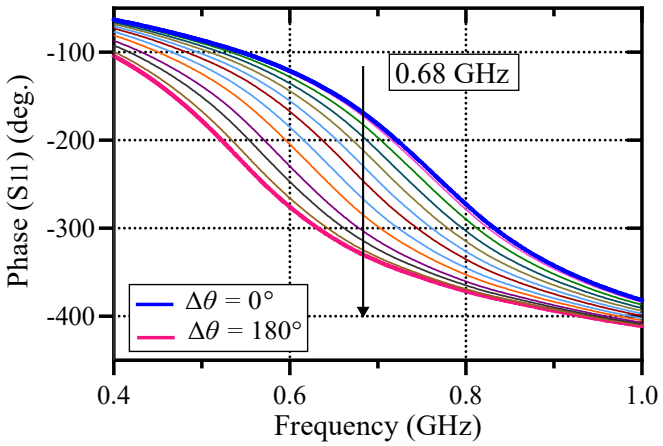

Fig. 11. The measured S_{11} phase for the fabricated rotation sensor, for different rotations from $0°$ to $180°$ with the step size of $15°$.

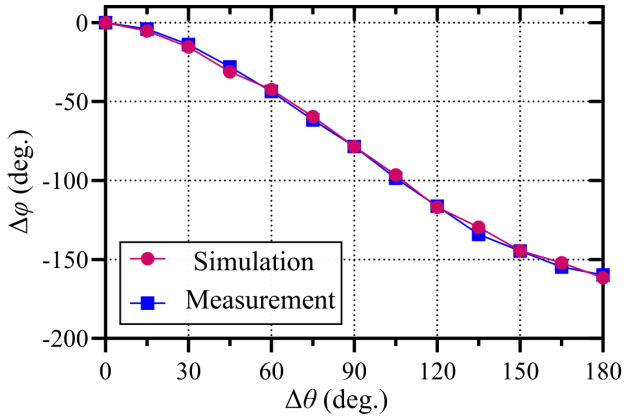

Fig. 12. Comparison of the simulation results and measured S_{11} phase variation of the the fabricated senosor, for different rotations from $0°$ to $180°$ with the step size of $15°$, measured at 0.68 GHz.

competitive sensitivity with respect to [58]. Our sensor offers the smallest electrical size among the others.

IV. CONCLUSION

A phase variation-based rotation sensor is designed and implemented in this paper. The sensor is modeled using an equivalent circuit and an analytical equation is derived using the circuit analysis for determining the frequency, which maximizes the sensitivity. Furthermore, a tapering method of the capacitive patch is introduced for linearizing the sensor response and avoiding the sensitivity saturation at large rotation angles. Based on the circuit analysis and the linearization method, a step-by-step procedure is developed for the design of a rotation sensor with a specified operation frequency (f). The proposed rotation sensing concept and the design procedure are verified by fabrication and measurement of a rotation sensor prototype operating at 0.68 GHz. The sensor performance has also been compared with the phase variation rotation sensors in the literature. The comparison show a very competitive performance with respect to the previously published works in the literature.

ACKNOWLEDGMENT

The authors would like to thank David Welch of RMIT University for his technical assistance in fabricating and assembling the sensor prototype.

REFERENCES

[1] N. Anandan and B. George, "A wide-range capacitive sensor for linear and angular displacement measurement," *IEEE Trans. Indust. Electron.*, vol. 64, no. 7, pp. 5728–5737, 2017.
[2] P. Hu, J. Guo, and J. Tan, "An annular planar-capacitive tilt sensor with a 360° measurement range," *IEEE Trans. Indust. Electron.*, vol. 63, no. 4, pp. 2469–2476, 2015.
[3] Z. Zhang, F. Ni, Y. Dong, C. Guo, M. Jin, and H. Liu, "A novel absolute magnetic rotary sensor," *IEEE Tran. Indust. Electron.*, vol. 62, no. 7, pp. 4408–4419, 2015.
[4] A. H. Karami, F. Karami Horestani, M. Kolahdouz, A. K. Horestani, and F. Martín, "2d rotary sensor based on magnetic composite of microrods," *Journal of Materials Science: Materials in Electronics*, vol. 31, no. 1, pp. 167–174, 2020.
[5] Y.-P. Yang and Y.-Y. Ting, "Improved angular displacement estimation based on hall-effect sensors for driving a brushless permanent-magnet motor," *IEEE Trans. Indust. Electron.*, vol. 61, no. 1, pp. 504–511, 2013.
[6] P. Pedersen, "Measurement, instrumentation, and sensors handbook. spatial, mechanical, thermal, and radiation measurement," 2014.
[7] T. A. Tameh, M. Sawan, and R. Kashyap, "Smart integrated optical rotation sensor incorporating a fly-by-wire control system," *IEEE Trans. Indust. Electron.*, vol. 65, no. 8, pp. 6505–6514, 2017.
[8] ——, "Novel analog ratio-metric optical rotary encoder for avionic applications," *IEEE Sens. Journal*, vol. 16, no. 17, pp. 6586–6595, 2016.
[9] J. Mata-Contreras, C. Herrojo, and F. Martin, "Application of split ring resonator (SRR) loaded transmission lines to the design of angular displacement and velocity sensors for space applications," *IEEE Trans. Microw. Theory Techn.*, vol. 65, no. 11, pp. 4450–4460, 2017.
[10] A. Ebrahimi, W. Withayachumnankul, S. F. Al-Sarawi, and D. Abbott, "Metamaterial-inspired rotation sensor with wide dynamic range," *IEEE Sensors Journal*, vol. 14, no. 8, pp. 2609–2614, 2014.
[11] J. Naqui, M. Duran-Sindreu, and F. Martín, "Alignment and position sensors based on split ring resonators," *Sensors*, vol. 12, no. 9, pp. 11 790–11 797, 2012.
[12] J. Naqui and F. Martín, "Angular displacement and velocity sensors based on electric-LC (ELC) loaded microstrip lines," *IEEE Sensors Journal*, vol. 14, no. 4, pp. 939–940, 2014.
[13] J. D. Baena, J. Bonache, F. Martín, R. M. Sillero, F. Falcone, T. Lopetegi, M. A. Laso, J. García-García, I. Gil, M. F. Portillo *et al.*, "Equivalent-circuit models for split-ring resonatorsand complementary split-ring resonators coupled to planar transmission lines," *IEEE Trans. Micrw. Theory Techn.*, vol. 53, no. 4, pp. 1451–1461, 2005.
[14] M. A. H. Ansari, A. K. Jha, and M. J. Akhtar, "Design and application of the CSRR-based planar sensor for noninvasive measurement of complex permittivity," *IEEE Sensors Journal*, vol. 15, no. 12, pp. 7181–7189, 2015.

[15] M. A. H. Ansari, A. K. Jha, Z. Akhter, and M. J. Akhtar, "Multi-band RF planar sensor using complementary split ring resonator for testing of dielectric materials," *IEEE Sensors Journal*, vol. 18, no. 16, pp. 6596–6606, 2018.

[16] A. Ebrahimi, J. Scott, and K. Ghorbani, "Dual-mode resonator for simultaneous permittivity and thickness measurement of dielectrics," *IEEE Sensors Journal*, vol. 20, no. 1, pp. 185–192, 2020.

[17] P. K. Varshney and M. J. Akhtar, "Substrate integrated waveguide derived novel two-way rotation sensor," *IEEE Sensors Journal*, vol. 21, no. 2, pp. 1519–1526, 2021.

[18] C. G. Juan, E. Bronchalo, B. Potelon, C. Quendo, E. Avila-Navarro, and J. M. Sabater-Navarro, "Concentration measurement of microliter-volume water–glucose solutions using Q factor of microwave sensors," *IEEE Trans. Instrum. Meas.*, vol. 68, no. 7, pp. 2621–2634, 2019.

[19] M. U. Memon, A. Salim, H. Jeong, and S. Lim, "Metamaterial inspired radio frequency-based touchpad sensor system," *IEEE Trans. Instrum. Meas.*, vol. 69, no. 4, pp. 1344–1352, 2020.

[20] S. Harnsoongnoen, "Metamaterial-inspired microwave sensor for detecting the concentration of mixed phosphate and nitrate in water," *IEEE Trans. Instrum. Meas.*, vol. 70, pp. 1–6, 2021.

[21] K. Grenier, D. Dubuc, T. Chen, F. Artis, T. Chretiennot, M. Poupot, and J.-J. Fournie, "Recent advances in microwave-based dielectric spectroscopy at the cellular level for cancer investigations," *IEEE Trans. Micrw. Theory Techn.*, vol. 61, no. 5, pp. 2023–2030, 2013.

[22] H.-J. Lee, J.-H. Lee, H.-S. Moon, I.-S. Jang, J.-S. Choi, J.-G. Yook, and H.-I. Jung, "A planar split-ring resonator-based microwave biosensor for label-free detection of biomolecules," *Sensors and Actuators B: Chemical*, vol. 169, pp. 26–31, 2012.

[23] Z. Abbasi, P. Shariaty, M. Nosrati, Z. Hashisho, and M. Daneshmand, "Dual-band microwave circuits for selective binary gas sensing system," *IEEE Trans. Micrw. Theory Techn.*, vol. 67, no. 10, pp. 4206–4219, 2019.

[24] M. H. Zarifi, P. Shariaty, Z. Hashisho, and M. Daneshmand, "A non-contact microwave sensor for monitoring the interaction of zeolite 13X with CO2 and CH4 in gaseous streams," *Sensors and Actuators B: Chemical*, vol. 238, pp. 1240–1247, 2017.

[25] H. El Matbouly, N. Boubekeur, and F. Domingue, "Passive microwave substrate integrated cavity resonator for humidity sensing," *IEEE Trans. Micrw. Theory Techn.*, vol. 63, no. 12, pp. 4150–4156, 2015.

[26] J. George, A. Abdelghani, P. Bahoumina, O. Tantot, D. Baillargeat, K. Frigui, S. Bila, H. Hallil, and C. Dejous, "CNT-based inkjet-printed RF gas sensor: Modification of substrate properties during the fabrication process," *Sensors*, vol. 19, no. 8, p. 1768, 2019.

[27] A. Salim and S. Lim, "Complementary split-ring resonator-loaded microfluidic ethanol chemical sensor," *Sensors*, vol. 16, no. 11, p. 1802, 2016.

[28] P. Vélez, J. Muñoz-Enano, K. Grenier, J. Mata-Contreras, D. Dubuc, and F. Martín, "Split ring resonator-based microwave fluidic sensors for electrolyte concentration measurements," *IEEE Sensors Journal*, vol. 19, no. 7, pp. 2562–2569, 2018.

[29] C. Drexler, T. V. Shishkanova, C. Lange, S. N. Danilov, D. Weiss, S. D. Ganichev, and V. M. Mirsky, "Terahertz split-ring metamaterials as transducers for chemical sensors based on conducting polymers: a feasibility study with sensing of acidic and basic gases using polyaniline chemosensitive layer," *Microchimica Acta*, vol. 181, no. 15-16, pp. 1857–1862, 2014.

[30] N. Sharafadinzadeh, M. Abdolrazzaghi, and M. Daneshmand, "Investigation on planar microwave sensors with enhanced sensitivity from microfluidic integration," *Sensors and Actuators A: Physical*, vol. 301, 2020, Art. no. 111752.

[31] M. Baghelani, N. Hosseini, and M. Daneshmand, "Artificial intelligence assisted non-contact microwave sensor for multivariable biofuel analysis," *IEEE Trans. Ind. Electron.*, vol. 68, pp. 11 492 – 11 500, 2020.

[32] S. Srisai and S. Harnsoongnoen, "Noncontact planar microwave sensor for liquid interface detection by a pixelated CSRR -loaded microstrip line," *International Journal of RF and Microwave Computer-Aided Engineering*, vol. 31, no. 4, 2021.

[33] A. Ebrahimi, F. J. Tovar-Lopez, J. Scott, and K. Ghorbani, "Differential microwave sensor for characterization of glycerol–water solutions," *Sensors and Actuators B: Chemical*, vol. 321, 2020, Art. no. 128561.

[34] A. K. Horestani, C. Fumeaux, S. Al-Sarawi, and D. Abbott, "Displacement sensor based on diamond-shaped tapered split ring resonator," *IEEE Sensors Journal*, vol. 13, no. 4, pp. 1153–1160, 2013.

[35] Z. Mehrjoo, A. Ebrahimi, and K. Ghorbani, "Phase variation reflective-mode displacement sensor using a CPW loaded with dumbbell-shaped resonator," in *IEEE Asia-Pacific Microwave Conference (APMC)*, 2021, DOI: 10.1109/APMC52720.2021.9661714.

[36] ——, "Microwave resonance-based reflective mode displacement sensor with wide dynamic range," *IEEE Trans. on Instum and Meas.*, vol. 71, 2021, Art. no: 8000609.

[37] J. Mata-Contreras, C. Herrojo, and F. Martin, "Detecting the rotation direction in contactless angular velocity sensors implemented with rotors loaded with multiple chains of resonators," *IEEE Sensors Journal*, vol. 18, no. 17, pp. 7055–7065, sep 2018.

[38] A. K. Jha, N. Delmonte, A. Lamecki, M. Mrozowski, and M. Bozzi, "Design of microwave-based angular displacement sensor," *IEEE Microwave and Wireless Components Letters*, vol. 29, no. 4, pp. 306–308, 2019.

[39] C. H. Chio, R. Gomez-Garcia, L. Yang, K. W. Tam, W.-W. Choi, and S. K. Ho, "An angular displacement sensor based on microwave transversal signal interference principle," *IEEE Sensors Journal*, vol. 20, no. 19, pp. 11 237–11 246, 2020.

[40] C.-H. Chio, R. Gomez-Garcia, L. Yang, K.-W. Tam, W.-W. Choi, and S.-K. Ho, "An angular-displacement microwave sensor using an unequal-length-bi-path transversal filtering section," *IEEE Sensors Journal*, vol. 20, no. 2, pp. 715–722, 2020.

[41] Y. Ding, C.-S. Lee, Y. Li, Z.-Q. Wang, and G.-F. Li, "An angular displacement sensor-based active feedback open complementary split-ring resonator," *IEEE Microwave and Wireless Components Letters*, vol. 31, no. 9, pp. 1079–1082, sep 2021.

[42] A. K. Jha, A. Lamecki, M. Mrozowski, and M. Bozzi, "A microwave sensor with operating band selection to detect rotation and proximity in the rapid prototyping industry," *IEEE Trans on Ind. Electron.*, vol. 68, no. 1, pp. 683–693, 2021.

[43] A. M. Gargari, B. Ozbey, H. V. Demir, A. Altintas, U. Albostan, O. Kurc, and V. B. Erturk, "A wireless metamaterial-inspired passive rotation sensor with submilliradian resolution," *IEEE Sensors Journal*, vol. 18, no. 11, pp. 4482–4490, 2018.

[44] J. Naqui and F. Martín, "Transmission lines loaded with bisymmetric resonators and their application to angular displacement and velocity sensors," *IEEE Trans. Micrw. Theory Techn.*, vol. 61, no. 12, pp. 4700–4713, 2013.

[45] J. Naqui, J. Coromina, A. Karami-Horestani, C. Fumeaux, and F. Martín, "Angular displacement and velocity sensors based on coplanar waveguides (CPWs) loaded with s-shaped split ring resonators (S-SRR)," *Sensors*, vol. 15, no. 5, pp. 9628–9650, 2015.

[46] Z. Shaterian, A. K. Horestani, and C. Fumeaux, "Rotation sensing based on the symmetry properties of an open-ended microstrip line loaded with a split ring resonator," in *proceedings of German Microwave Conference*, 2015, pp. 33–35.

[47] A. K. Horestani, D. Abbott, and C. Fumeaux, "Rotation sensor based on horn-shaped split ring resonator," *IEEE Sensors Journal*, vol. 13, no. 8, pp. 3014–3015, 2013.

[48] J. Coromina, J. Muñoz-Enano, P. Vélez, A. Ebrahimi, J. Scott, K. Ghorbani, and F. Martín, "Capacitively-loaded slow-wave transmission lines for sensitivity improvement in phase-variation permittivity sensors," in *50th European Microwave Conference (EuMC)*, 2020, pp. 491–494.

[49] J. Muñoz-Enano, P. Vélez, L. Su, M. Gil-Barba, and F. Martín, "A reflective-mode phase-variation displacement sensor," *IEEE Access*, vol. 8, pp. 189 565–189 575, 2020.

[50] J. Muñoz-Enano, P. Casacuberta, L. Su, P. Vélez, M. Gil, and F. Martín, "Open-ended-line reflective-mode phase-variation sensors for dielectric constant measurements," *IEEE Sensors Conference*, 2020, DOI: 10.1109/SENSORS47125.2020.9278857.

[51] J. Muñoz-Enano, P. Vélez, L. Su, M. Gil, P. Casacuberta, and F. Martín, "On the sensitivity of reflective-mode phase-variation sensors based on open-ended stepped-impedance transmission lines: Theoretical analysis and experimental validation," *IEEE Trans. Micrw. Theory Techn.*, vol. 69, no. 1, pp. 308–324, 2020.

[52] L. Su, J. Muñoz-Enano, P. Vélez, C. Pau, M. Gil-Barba, and F. Martín, "Highly sensitive phase variation sensors based on step-impedance coplanar waveguide (CPW) transmission lines," *IEEE Sensors Journal*, vol. 21, no. 3, pp. 2864–2872, 2020.

[53] L. Su, J. Muñoz-Enano, P. Vélez, M. Gil-Barba, P. Casacuberta, and F. Martín, "Highly sensitive reflective-mode phase-variation permittivity sensor based on a coplanar waveguide terminated with an open complementary split ring resonator (OCSRR)," *IEEE Access*, vol. 9, pp. 27 928–27 944, 2021.

[54] P. Casacuberta, J. Muñoz-Enano, P. Vélez, L. Su, M. Gil, and F. Martín, "Highly sensitive reflective-mode defect detectors and dielectric constant sensors based on open-ended stepped-impedance transmission lines," *Sensors*, vol. 20, no. 21, 2020, Art. no. 6236.

[55] A. K. Horestani, Z. Shaterian, and F. Martín, "Rotation sensor based

on the cross-polarized excitation of split ring resonators (SRRs)," *IEEE Sensors Journal*, vol. 20, no. 17, pp. 9706–9714, 2020.
[56] A. Ebrahimi, J. Coromina, J. Muñoz-Enano, P. Vélez, J. Scott, K. Ghorbani, and F. Martín, "Highly sensitive phase-variation dielectric constant sensor based on a capacitively-loaded slow-wave transmission line," *IEEE Trans. Circ. Syst. I*, vol. 68, no. 7, pp. 2787–2799, 2021.
[57] A. K. Horestani, Z. Shaterian, and M. Mrozowski, "High dynamic range microwave displacement and rotation sensors based on the phase of transmission in groove gap waveguide technology," *IEEE Sensors Journal*, vol. 22, no. 1, pp. 182–189, 2022.
[58] A. K. Jha, A. Lamecki, M. Mrozowski, and M. Bozzi, "A highly sensitive planar microwave sensor for detecting direction and angle of rotation," *IEEE Transactions on Microwave Theory and Techniques*, vol. 68, no. 4, pp. 1598–1609, 2020.
[59] P. Vélez, J. Mñnoz-Enano, A. Amir Ebrahimi, C. Herrojo, F. Paredes, J. Scott, K. Ghorbani, and F. Martín, "Single-frequency amplitude-modulation sensor for dielectric characterization of solids and microfluidics," *IEEE Sensors Journal*, vol. 21, no. 10, pp. 12 189–12 201, 2021.
[60] J. Muñoz-Enano, J. Martel, P. Vélez, F. Medina, L. Su, and F. Martín, "Parametric analysis of the edge capacitance of uniform slots and application to frequency-variation permittivity sensors," *Applied Sciences*, vol. 11, no. 15, 2021, art. no.: 7000.

Zahra Mehrjoo (Graduate Student Member, IEEE) received her B.Sc. degree in electrical and electronic engineering and the M.Sc. degree in Microelectronics from Shiraz University of Technology, Shiraz, Iran in 2009 and 2012, respectively. Her research interests include RF microelectronics, metamaterial inspired microwave devices, and microwave circuit design and analysis. Currently, she is pursuing her Ph.D. degree at RMIT university, Melbourne, Australia with a focus on the development of metamaterials-inspired microwave sensors for mechanical displacement, rotation, and materials characterization.

Amir Ebrahimi (S'09, M'16) received the B.Sc. degree in electrical engineering in 2008, the M.Sc. degree in microelectronics in 2011, and the Ph.D. degree from the University of Adelaide, Adelaide, Australia in 2016. He is now a research fellow in the School of Engineering, RMIT University, Melbourne, Australia.

He was a Visiting Research Fellow at Nanyang Technological University (NTU), Singapore, during 2014-2015. His research interests include metamaterial inspired microwave devices, microwave circuit design, microwave filters, frequency-selective surfaces (FSSs) and nonlinear RF, and microwave circuits design and analysis.

Dr. Ebrahimi was a recipient of the Australian National Fabrication Facility (ANFF) Award (2013), the University of Adelaide D.R. Stranks Traveling Fellowship (2014), the Yarman-Carlin Best Student Paper Award at the Mediterranean Microwave Symposium (2015), the Simon Rockliff Scholarship (2016), the Best Paper award at the Australian Microwave Symposium (2016), Gertrude Rohan Memorial Prize (2017), the CASS Foundation travel award (2019), Best Young Investigator Paper Award, MTT Section, Australian Microwave Symposium (2020). He is a reviewer for several recognized international journals such as IEEE TRANSACTIONS ON MICROWAVE THEORY AND TECHNIQUES, IEEE TRANSACTIONS ON ANTENNAS AND PROPAGATIONS, and IEEE MICROWAVE AND WIRELESS COMPONENTS LETTERS.

Grzegorz Beziuk (M'19) was born in Wrocław, Poland, in 1974. He received the M. Sc. Eng. and Ph.D. degrees in electronics and telecommunication from the Wrocław University of Science and Technology, Wrocław, in 1999 and 2005, respectively. From February 1999 to December 2013, he was appointed as a Research Assistant, a Lecturer, and an Assistant Professor with the Faculty of Electronics, Wrocław University of Technology, Wrocław. In January 2014, he joined the Mass Spectrometry Laboratory, Department of Physics, The University of Auckland, Auckland, New Zealand, as a Research Engineer. From July 2015 to May 2018, he was a Process and Test Engineer with the TriCab Pty. Ltd. Group, Melbourne, VIC, Australia. In June 2018, he joined the Royal Melbourne Institute of Technology, Melbourne, as a Research Fellow. He successfully collaborated with many industrial partners and scientific institution, notably CERN, Geneva, Switzerland and GSI, Darmstadt, Germany, where he was working on fault diagnostics of superconducting and normal conducting magnets of LHC and FAIR particle accelerators. His current research interests include electronic circuits, microwaves and THz techniques, RF circuit fabrication methods, instrumentation and measurement techniques, and electromagnetic (EM) geophysical methods.

Ferran Martín (M'04-SM'08-F'12) was born in Barakaldo, Spain, in 1965. He received the B.S. degree in physics and Ph.D. degree from the Universitat Autònoma de Barcelona (UAB), Barcelona, Spain, in 1988 and 1992, respectively. From 1994 to 2006 he was Associate Professor in Electronics at the Departament d'Enginyeria Electrònica (Universitat Autònoma de Barcelona), and since 2007 he is Full Professor of Electronics. His research activity has been very broad, including the modelling and simulation of electron devices for high frequency applications, millimeter wave and THz generation systems, the application of electromagnetic bandgaps to microwave and millimeter wave circuits, and the application of metamaterial concepts to the miniaturization and optimization of microwave circuits and antennas. He is now very active in the development of microwave sensors for dielectric characterization and motion control, and also in the topic of chipless-RFID. He is the head of the Microwave Engineering, Metamaterials and Antennas Group (GEMMA Group) at UAB, and director of CIMITEC, a research Center on Metamaterials supported by TECNIO (Generalitat de Catalunya). He has organized several international events related to metamaterials, including Workshops at the IEEE International Microwave Symposium (years 2005 and 2007) and European Microwave Conference (years 2009, 2015, 2017, and 2018), and the Fifth International Congress on Advanced Electromagnetic Materials in Microwaves and Optics (Metamaterials 2011), where he has acted as chair of the Local Organizing Committee. He has acted as Guest Editor in several Special Issues, mainly related to Metamaterials, in various International Journals. He has authored and co-authored over 600 technical conference, letter, journal papers and book chapters, he is co-author of the book on Metamaterials entitled *Metamaterials with Negative Parameters: Theory, Design and Microwave Applications* (John Wiley & Sons Inc. 2008), author of the book *Artificial Transmission Lines for RF and Microwave Applications* (John Wiley & Sons Inc. 2015), co-editor of the book *Balanced Microwave filters* (John Wiley & Sons Inc. and IEEE-Press 2018), and co-author of the book *Time Domain Signature Barcodes for Chipless-RFID and Sensing Applications* (Springer, 2020). Ferran Martín has generated 21 PhDs, has filed several patents on metamaterials and related concepts, and has headed several development contracts.

Prof. Martín is a member of the IEEE Microwave Theory and Techniques Society (IEEE MTT-S), member of the European Microwave Association (EuMA), and member of the Institution of Electronics and Technology (IET). He is reviewer of dozens of journals, including IEEE journals such as IEEE TRANSACTIONS ON MICROWAVE THEORY AND TECHNIQUES, IEEE MICROWAVE AND WIRELESS COMPONENTS LETTERS, and IEEE SENSORS JOURNAL, among others, and he serves as member of the Editorial Board of IET Microwaves, Antennas and Propagation and International Journal of RF and Microwave Computer-Aided Engineering. He is also a member of the Technical Committees of the European Microwave Conference (EuMC) and International Congress on Advanced Electromagnetic Materials in Microwaves and Optics (Metamaterials). Among his distinctions, Ferran Martín has received the 2006 Duran Farell Prize for Technological Research, he holds the *Parc de Recerca UAB – Santander* Technology Transfer Chair, and he has been the recipient of three ICREA ACADEMIA Awards (calls 2008, 2013 and 2018). He is Fellow of the IEEE since 2012 and Fellow of the IET since 2016.

Kamran Ghorbani (M'96, SM'17) received the B.Eng (Hons.) and a Ph.D. degree from RMIT University, Melbourne, VIC, Australia, in 1994 and 2001, respectively. From Nov. 1994 to 1996, he was a graduate RF Engineer with AWA Defence Industries working on early warning radar systems. In June 1996, he joined RMIT University to pursue his PhD studies. From Dec. 1999 to March 2001, he was a Senior RF Engineer with Tele-IP working on VHF transceivers for commercial aircraft. He joined the Department of Communication and Electronic Engineering (now the School of Engineering) at RMIT University in 2001 as a continuing Academic.

Prof. Ghorbani is currently Director of the Communication Technologies Research Centre, RMIT University. He is responsible for strategic planning and managing the research center. His research interests include dielectric measurements, composite material structures, frequency selective surfaces, metamaterials, RF energy harvesting, radar systems, ferroelectric devices and multifunctional antennas.

Prof. Ghorbani was the Chair of Asia Pacific Microwave Conference APMC2011, Melbourne, Australia. He was the Co-Chair of Technical Program Committee for the IEEE International Microwave and RF Conference, IMaRC2014, India. He was the Chair of first Australian Microwave Symposium, AMS2014, Melbourne, Australia. He was the Chair of Technical Program Committee of the Asia Pacific Microwave Conference APMC2016, India.

He served as an Associate Editors of IEEE TRANSACTIONS ON MICROWAVE THEORY AND TECHNIQUES, and IET Microwaves, Antennas & Propagation. He is a voting member of IEEE MTT-S Administrative Committee.